Lattice dynamics localization in low-angle twisted bilayer graphene

Andreij C. Gadelha,[1] Douglas A. A. Ohlberg,[1] Cassiano Rabelo,[2] Eliel G. S. Neto,[3] Thiago L. Vasconcelos,[4] João L. Campos,[1] Jessica S. Lemos,[1] Vinícius Ornelas,[1] Daniel Miranda,[1] Rafael Nadas,[1] Fabiano C. Santana,[1] Kenji Watanabe,[5] Takashi Taniguchi,[5] Benoit van Troeye,[6] Michael Lamparski,[6] Vincent Meunier,[6] Viet-Hung Nguyen,[7] Dawid Paszko,[7] Jean-Christophe Charlier,[7] Leonardo C. Campos,[1] Luiz G. Cançado,[1] Gilberto Medeiros-Ribeiro,[8] and Ado Jorio[1,2]

[1]*Physics Department, Universidade Federal de Minas Gerais, Belo Horizonte, MG 31270-901, Brazil.*

[2]*Electrical Engineering Graduate Program, Universidade Federal de Minas Gerais, Belo Horizonte, MG 31270-901, Brazil.*

[3]*Physics Institute, Universidade Federal da Bahia, Campus Universitário de Ondina, Salvador - BA, 40170-115 Brazil.*

[4]*Divisão de Metrologia de Materiais, Inmetro, Duque de Caxias, RJ 25250-020 Brazil.*

[5]*National Institute for Materials Science (NIMS), 1-2-1 Sengen, Tsukuba-city, Ibaraki 305-0047, Japan.*

[6]*Physics, Applied Physics, and Astronomy, Jonsson Rowland Science Center, Room 1C25 110 8th Street Troy, NY 12180, USA.*

[7]*Institute of Condensed Matter and Nanosciences (IMCN) University of Louvain (UCLouvain), Louvain-la-Neuve, Belgium.*

[8]*Computer Science Department, Universidade Federal de Minas Gerais, Belo Horizonte, MG 31270-901, Brazil.*

(Dated: October 2, 2020)

A small twist angle between the two stacked crystal networks in bilayer graphene enables self-organized lattice reconstruction with the formation of a periodically repeated domain [1–3]. This superlattice modulates the vibrational [3, 4] and electronic [5, 6] structures, imposing new rules for electron-phonon coupling [7, 8] and the observation of strong correlation and superconductivity [9]. Here we report the direct observation of hyperspectral optical images of the crystal superlattice in reconstructed twisted bilayer graphene, generated by the inelastic scattering of light in a nano-Raman spectroscope [10]. The observation of the crystallographic structure with visible light is made possible by the lattice dynamics localization with image formation due to spectral variations caused by the presence of strain solitons and topological points [1]. The results are rationalized by an atomistic model that allows for unfolding the tens of thousands of phononic bands on fully-relaxed structures of the large unit cell. This procedure enables the evaluation of local density of vibrational states that, along with electronic properties of the same relaxed structures, highlights the relevance of solitons and topological points, particularly pronounced for structures with small twist angles. We anticipate this discovery to play a significant role in understanding Jahn-Teller effects [11] and electronic Cooper pairing [12–14], among many other important phonon-related effects at the atomic and nanoscales, and it is poised to enable important development in the characterization of devices [15] in the framework of the fast-developing field of twistronics [16].

Graphite lattice dynamics have been widely studied for engineering the broadly utilized thermal and electrical properties of this semi-metal [17]. Bilayer graphene, which in the so-called AB Bernal stacking represents the basic two-dimensional unit to build three-dimensional graphite, has recently gained great attention because of its rich structural and electronic behavior when arranged with a small relative twist angle θ between the two layers. Below a threshold twist angle $\theta_c \sim 1^\circ$, twisted bilayer graphene (TBG) undergoes an energetically favorable atomic reconstruction, entering the soliton regime for $\theta < \theta_c$ [3, 18]. This equilibrium configuration possesses alternating AB and BA triangular stacking domains separated by shear solitons representing saddle-points (SP) of the van der Waals energy landscape [1] in the hexagonal network [1, 18], with AA-stacked topological regions composing the vertices of the triangular areas (see Fig. 1**a**). This reconstructed twisted bilayer graphene

(rTBG) is a novel material system, where emerging local phenomena related to electronic and phononic reconstructions in addition to the morphology rearrangement [6, 18] are yet to be fully understood.

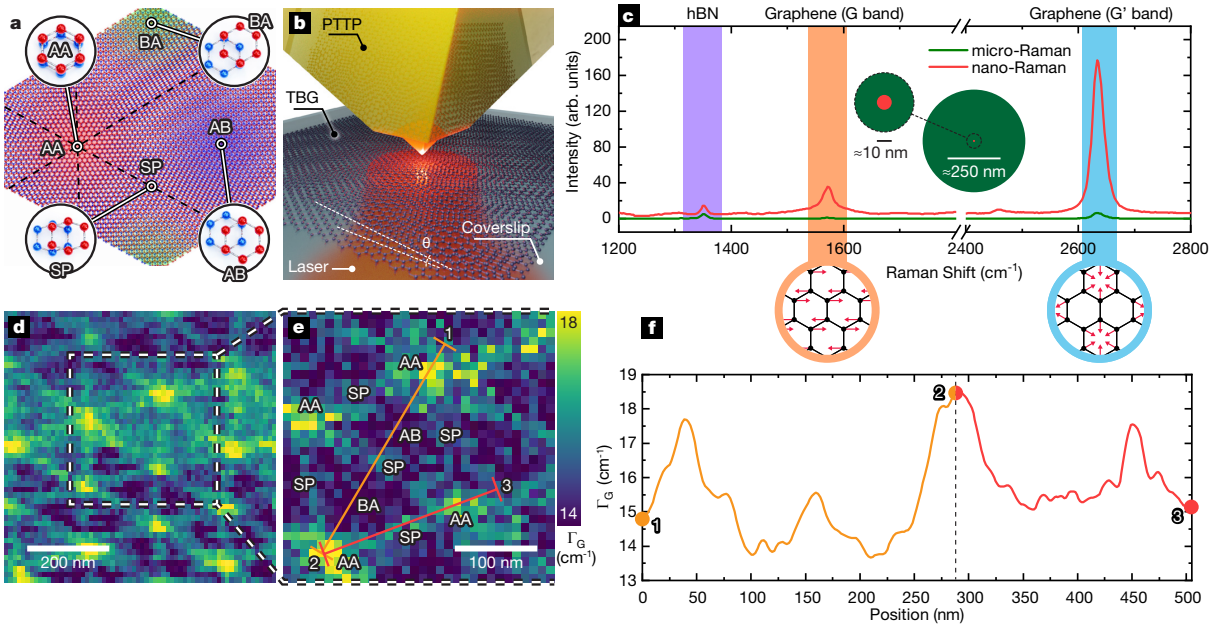

FIG. 1. **Nano-Raman spectral imaging of a crystallographic superlattice in reconstructed twisted bilayer graphene**. **a** Schematics showing neighbouring AB and BA-stacked domains, strain solitons (saddle-points - SP), and topological points (AA). **b** Schematics of the plasmon-tunable tip pyramid nano-antenna responsible for the enhancement of the Raman signal in a nanometric area, in the tip-enhanced Raman spectroscopy (TERS) configuration. **c** Comparison between micro-Raman (green) and the nano-Raman (red) spectra in the sample (an enlarged version of the green spectrum can be found in the supplementary information). Green and red circles indicate the different illumination areas. The G and G′ vibrational modes are depicted, as well as the peak from the hBN substrate. The G′ branch is also named $2D$ in the literature. **d** Crystallographic hyperspectral image of a reconstructed twisted bilayer graphene based on the G′ band nano-Raman intensity; **e** Zoomed-in image from **b** based on the G band nano-Raman linewidth (Γ_G). **f** Line profile for Γ_G along the high symmetry directions shown by the orange and red lines in **e**. The data is averaged over the pixels delimited by the ending bars in those lines.

Experimentally, Raman spectroscopy, the inelastic scattering of light, remains a key technique to study the vibrational structure of graphite-related systems [19], even gaining fur-

ther importance for low-dimensional structures [20, 21], where inelastic neutron or X-ray scattering are difficult to use. To visualize the detailed structure of rTBG, however, a nano-Raman spectroscope, capable of resolving the optical information below the light diffraction limit (Figs. 1**b**,**c**), is necessary [10]. Figures 1**d**-**f** reveal a nano-Raman imaging of solitonic arrangements in a rTBG with $L_M = 160 \pm 30\,\mathrm{nm}$ superlattice periodicity, which corresponds to $\theta = 0.09 \pm 0.02°$, using $L_M = a_0/2\sin(\theta/2)$ with graphene lattice parameter $a_0 = 0.245 \pm 0.001\,\mathrm{nm}$. The specific nano-antenna of our nano-Raman setup, a plasmon-tunable tip pyramid [22] shown schematically in Fig. 1**b**, is crucial for the acquisition of the images reproduced in Figures 1**d**,**e**. It yields a local signal enhancement on the order of 3×10^3, thus generating a nano-Raman signal so intense that the micro-Raman response from the micron-sized illumination area becomes negligible (see Fig. 1**c**). The nano-Raman images are obtained at ambient conditions over regions of the bilayer that appear atomically flat and featureless in the surface topology images simultaneously obtained by the nano-antenna, which also functions as an atomic force microscope probe. Extremely clean rTBG samples without a top, capping hBN flake are also essential for high quality nano-Raman data. To produce such samples, we developed a new dry tear-and-stack method [23], based on a semi-pyramidal stamp that allows the preparation of high-quality TBG flakes on a glass coverslip. These samples were extensively characterized by scanning probe microscopy techniques (SPM), including atomic force microscopy (AFM), scanning microwave impedance microscopy (sMIM), and scanning tunneling microscopy (STM).

The particular configuration shown in Fig. 1**d** was observed previously by transmission electron microscopy (TEM) [1, 3, 4] and nano-infrared spectroscopy [24] techniques. The authors of these studies attribute the solitonic structure and soliton interceptions to shear strain solitons and topological AA points, respectively, based on the similarity between the observed superlattices and theoretical expectations for TBG reconstruction at low twist angles (see schematics in Fig. 1**a**). Here, the superlattice imaging is directly related to the distribution of local vibrational states and electronic rTBG structure, since the nano-Raman spectroscopy probes the local atomic lattice vibration directly. The main Raman spectral signatures in graphene are due to the stretching of the C-C bonds (conventionally named G band, appearing at 1584 cm^{-1}) and the breathing motion of the hexagonal carbon rings (named G′ band, symmetry-allowed overtone appearing at 2640 cm^{-1}), as assigned in Fig. 1**e**. Fig. 1**d** is a hyperspectral image based on the intensity of the rTBG Raman G′ band, while

Fig. 1**e** is a zoomed-in region of Fig. 1**d** based on the linewidth (Γ_G) of the Raman G band. Note that in these images, the data-sets were plotted in their raw forms, *i.e.*, without any statistical treatment or data filtering.

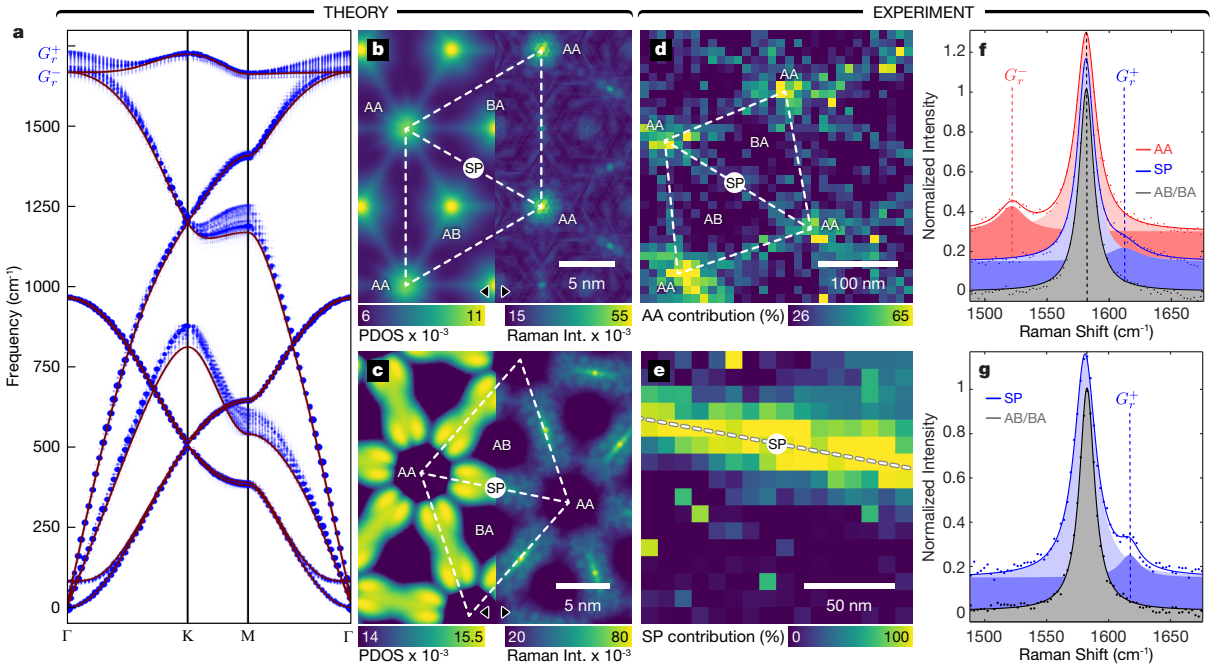

FIG. 2. **Phonon structure and the nano-Raman spectral signature**. **a** Theoretical phonon dispersion for Bernal AB-stacked bilayer graphene (red) and for reconstructed twisted bilayers graphene (blue). The band structure for the rTBG was obtained by unfolding the phonon bands of the small Brillouin zone (BZ) of the superlattice onto the much larger BZ of graphene. The frequency degeneracy at the Γ point between the AB-stacked phonon (red) and lower branch rTBG (blue) may be lifted due to different electron-phonon interactions, which are not considered in these calculations. **b** and **c** are the theoretically predicted spatial distributions of the phonon density of states (PDOS, left) and Raman intensity (right) for the lower (G_r^-) and higher (G_r^+) frequency optical phonons at the Γ point, respectively. **b** and **c** are different in size and position with respect to each other, for better correlation to **d** and **e**. **d** and **e** are the experimentally measured hyperspectral mapping of the AA and SP Raman spectra, as defined in **f** and **g**, respectively (the contribution renders their respective spectral weight, as defined in the Methods). Data in **d**,**f** comes from the same location as in Fig.1**c**.

The specific vibrational modes for the G and G′ Raman bands (see inset to Fig. 1**c**) are not only different, but the scattering mechanisms that are responsible for these Raman

features [20, 21] differ, as well. The G band is a first-order Raman active mode related to the doubly-denegerated high-frequency optical phonon branch in graphene at the Brillouin zone center (Γ point, see red lines in Fig. 2**a**). While the Bernal-stacked bilayer graphene exhibits a single Raman-active phonon band (red G), the rTBG exhibits a splitting of the vibrations in several branches [6], two of which are predominant in the high-frequency at the Γ point. This splitting will be the focus of our attention in the following discussion. Previous models for twisted bilayer graphene [7] cannot explain this splitting because these phonon branches result from atomic reconstruction with the emergence of topological solitons. In stark departure from results previously reported in the literature, our methodology allows for unfolding the tens of thousands of phononic bands of the large rTBG unit cell into those of graphene, thus making it possible to monitor how graphene's intrinsic phonon properties evolve when relaxing into the rTBG structure. We show an example of the resulting (unfolded) band-structure in Fig. 2**a** for a rTBG (blue lines) with a twist angle of 0.987°. In addition, we show in the left half of Fig. 2**b** and Fig. 2**c** the local phonon density of states around the lower phonon branch (G_r^-) and the higher phonon branch (G_r^+), respectively, another specificity of our fully atomistic model, which allows the analysis of localized projected density of phononic states in AA, AB/BA and SP stacking regions. These modes are, therefore, predicted to be localized in space, the lower frequency mode G_r^- appearing more strongly on the AA regions and at the very center of the AB/BA domains, and the higher frequency mode preferentially in the SP regions.

A close inspection of the experimental Raman data shows the appearance of two satellite peaks next to the G band, also named here G_r^+ and G_r^-, appearing above and below the G band, respectively. Remarkably, they are localized in space exactly as predicted by theory (see Figs. 2**b,d** and **c,e**). The Raman intensity is not only defined by the phonon density of states, but it also depends on the electron-phonon coupling, and the absence of an experimental contribution from G_r^- at the center of the AB/BA domains (compare Figs. 2**b**,**d**) is in agreement with the Raman intensities we computed using the bond polarizability model [25], as displayed in the right half of Figs. 2**b** and **c** (details in the supplementary information). ~~Notice also that the most intense G band is never predicted to disappear, being observable all over the rTBG sample.~~ The G band itself is reminiscent of the unfolded structure, partially contaminated by Bernal stacked data because of the limited TERS resolution, but also exhibiting local information, as clearly evidenced by the change in linewidth shown in

Fig.1**e**,**f**.

The remarkable result is that the theoretically predicted phonon localization, which cannot be accessed with usual continuous models, is consistent with the experimental nano-Raman results of highly-localized phonons in twisted bilayer graphene. Figures 2**d**,**f** are data from the same location used in Fig. 1**e**, and Fig. 2**d** shows the local contribution of the spectrum named AA, as defined in Fig. 2**f**. Fig. 2**e** is a higher resolution imaging of a single soliton to better evidence the SP spectra with the lower intensity G_r^+ peak, as shown in Fig. 2**g**. This data processing relied on the principal component analysis (PCA), as described in the Methods.

The frequency difference between the theoretically predicted G_r^- and G_r^+ peaks is 45 cm^{-1}, while for the experimentally observed G_r^- and G_r^+ peaks, it is 90 cm^{-1}. This splitting is predicted to increase with decreasing twist angle [6], consistent with the different twist angles in experiment ($\theta = 0.09°$) and calculations ($\theta = 0.987°$), the latter already reaching the limit of our computational capability. Note that in [6], the splitting was calculated between the maximal and minimal eigenvalues that feature prominently at Γ (yielding a value of 60 cm^{-1}), while here the value of 45 cm^{-1} was measured as the distance between the centre of the sub-bands. Our ability to experimentally define the θ-dependence of the splitting is also limited, but by our TERS resolution: we cannot properly image a moiré pattern smaller than 40 nm, limiting the rTBG we can image to those with $\theta < 0.3°$.

The G′ band, utilized to obtain Fig. 1**d**, is also related to the high-frequency optical phonon branch in graphene, but away from the Brillouin zone center, close to the K or K' points [20, 21, 26]. Figures 3**a** and **b** illustrate nano-Raman spectra observed at an AB/BA region and at an SP region, respectively. We see no clear distinction between the soliton and AA region spectral signatures. The spectrum shown in Fig. 3**a** is typical of a Bernal-stacked bilayer, depicting four Lorentzian peaks [27], thus confirming the AB-stacking structure, while the spectrum in Fig. 3**b** is different, displaying a unique shape for the SP/AA Raman signature. These spectral profiles were used to fit the G′ hyperspectra shown in Fig. 1, and the spectral weight of the AB/BA and SP/AA spectral information are plotted in Fig. 3**c** and Fig. 3**d**, respectively, evidencing clearly the rTBG structure.

The G′ lineshape is known to be sensitive to the electronic structure as it is mediated in part by electron-phonon coupling [20, 21, 26]. Moreover, the dependence on the number of Bernal-stacking layers [27] and on twist-angle [7] in bilayer has been established. Here, we

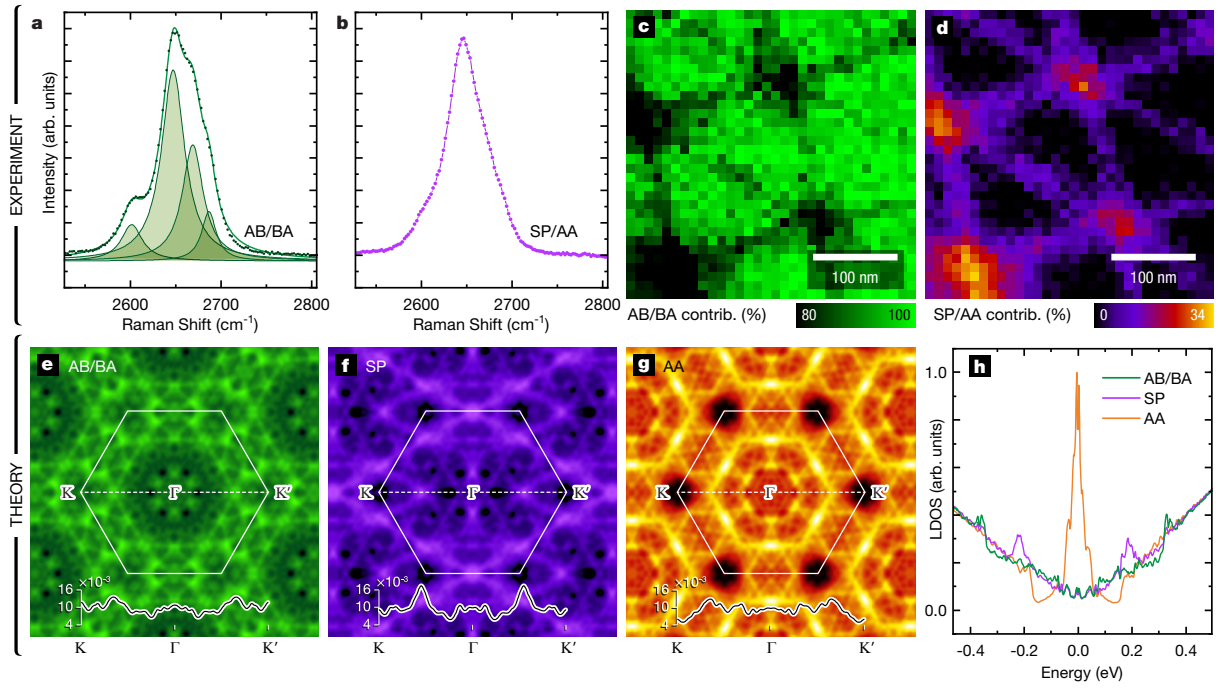

FIG. 3. **Nano-Raman spectral signature (upper line) and the electronic structure (lower line)**. **a** spectral Raman signature of the AB/BA-staked domains; **b** corresponding data for the SP/AA domains; **c** and **d** are the spectral weights for the AB and SP/AA signatures, respectively, in the rTBG real space (same location as in Fig.1**c**); **e** to **g** are the density of states at $E = -0.98\,\mathrm{eV}$, plotted in momentum space, for the AB/BA, SP and AA regions, respectively. The color map renders the DOS values, as shown by the insets with the line-trace for the DOS values along the K-Γ-K′ direction. The choices of (**e**) green, (**f**) purple and (**g**) orange make a connection to the respective real spatial locations in **c**,**d**. **h** DOS as a function of energy near the Fermi level for AB/BA, SP and AA regions.

show that in rTBG not only the phonon structure exhibits localization, but also the electronic structure, as shown in [18] and discussed in details in the supplementary information. As explained in Methods, our developed calculation techniques based on recursive Green's functions allow to compute highly accurate electronic models (i.e., atomistic tight-binding Hamiltonians taking into account the effects of structural relaxation). These calculations are not only tractable for very low twist angles but also allow for the detailed analysis of both global (dispersion relations and total DOS) and local electronic properties, thereby providing information that cannot be obtained using continuous models. Figures 3**e** to **g** illustrate

how the electronic density of states (DOS) in momentum space, at a fixed energy, changes locally in a typical low-angle rTBG system ($\theta = 0.505°$). Some other low-angle rTBG structures are also investigated and discussed in more details in Fig. S11 of the supplementary information. The fixed energy was chosen as $E_{DOS} = -0.98\,\text{eV}$, i.e., the energy for the valence electrons that are excited to the conduction band by our $E_L = 1.96\,\text{eV}$ excitation laser ($|E_{DOS}| = E_L/2$). Therefore, consistent with the non-local effect due to number of Bernal-stacking layers [27] or interlayer twist-angle [7], the changes in the electronic structure in rTBL are qualitatively reflected in the G′ band spectral signature locally, see Figures 3**a** to **d**. However, a clear quantitative analysis requires further theoretical developments for addressing the electron-phonon coupling in these complex systems.

While it is evident that strain plays a role in the observed Raman frequencies and linewidths in rTBG, this time-independent perturbation alone cannot explain the observed results, as evidenced by the Γ_G line-profile in Fig.1**f** and by a joint analysis of the G and G′ features, based on what has been established in the literature (details are provided as supplementary information) [28–30]. Aspects related to dynamic electron-phonon coupling, already proven to be very important in determining the phonon properties of graphene-related systems [31–34], including AB-staked bilayer graphene [35], have to be taken into account. In this sense, changes in local DOS for rTBG also take place near the Fermi level, as shown in Fig. 3**h** (see supplementary information for more details, including a localized joint DOS analysis), with further implications for the electron-phonon coupling and, consequently, for the nano-Raman imaging. G band phonons can be annihilated, generating an electron-hole pair, and this mechanism decreases the overall G phonon lifetime, thus broadening the G peak in the Raman spectrum [32, 33, 35]. A G band phonon carries an energy of $\hbar\omega_G \approx 0.2\,\text{eV}$. As a result, we expect that the presence of DOS peaks at $\pm 0.2\,\text{eV}$ from the Fermi level in Fig. 3**h**, which are found to be preserved even for smaller twisted angles, causes a broadening of the rTBG G band in the SP (green) and AA (blue) regions. These predictions agree with the results shown in Fig.1**e**,**f**, notably in the AA regions, where the G band is wider due to the DOS peak also at the Fermi level (see Fig. 3**h**). In addition, the widths of the G_r^- and G_r^+ peaks have been found in the range 26–30 cm^{-1} and 30–32 cm^{-1} (see additional data in the supplementary information), respectively, with the G_r^- always slightly sharper (2–4 cm^{-1}) than the G_r^+. These values may bring future insights into the real-space electron-phonon coupling, as these two modes are associated with regions with

different stacking order.

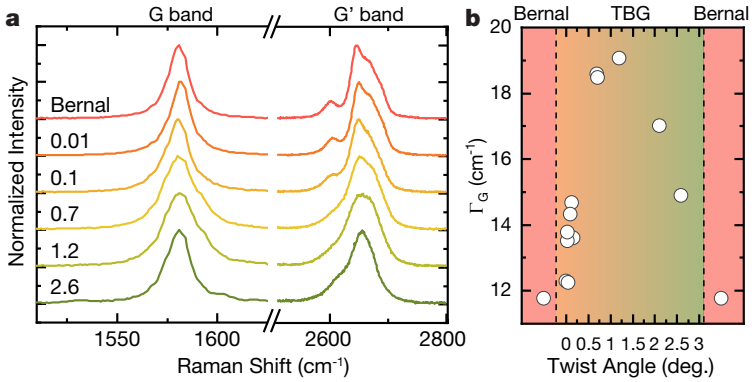

FIG. 4. **Micro-Raman spectral fingerprint for different twisted bilayer graphene at different twist angles.** **a** focuses on the G and G′ band spectra and **b** shows the full-width at half maxima of the G peak (Γ_G). The rTBG θ values were measured by high-resolution sMIM. The spectrum for Bernal AB-stacking was measured for reference.

Finally, to link the nano-Raman scattering experiments presented here with the usual micro-Raman spectroscopy characterization of twisted bilayer graphene, Fig. 4**a** shows the micro-Raman G and G′ spectra for different twist angles between 0.01 and 2.6 degrees. We also plot in Fig 4**a** the spectra for the Bernal-bilayer graphene, for reference, and Fig. 4**b** shows the full-width at half maximum (FWHM) for the observed G band (Γ_G). An increase of Γ_G when decreasing the twist angle below $\theta = 5°$ was reported [36], but here we see evidence that it reaches a maximum near the magic angle ($\theta \sim 1.1°$) [9], and it decreases for lower twist angle values, back to the reference Bernal AB-stacking value at $\Gamma_G = 12\,\mathrm{cm}^{-1}$ when $\theta \to 0$, see Fig. 4**b**. Considering reconstruction regime for $\theta < 1.2°$ [18], when the angle decreases, the ratio between the AA/SP and AB/BA areas decrease, and the TBG G band tends to the corresponding AB version, see Fig. 4**b**. It is interesting, however, to find Γ_G as high as $19\,\mathrm{cm}^{-1}$ near the magic angle, consistent with the Γ_G value observed at AA points in Fig. 1**e**,**f**. This value is higher than graphene at the charge neutrality point, where the electron-phonon coupling is maximum [32, 33]. As already pointed out, Γ_G is affected by both strain and the time-dependent perturbations related to the electron-phonon coupling [35, 37], and the Γ_G results here indicate a peak in the electron-phonon coupling near the magic angle, an evidence of the possible role of phonons in graphene superconductivity. We stress, however, that up to this point, the relation between Γ_G and the theoretical analysis of

strain and local DOS-based electron-phonon coupling is qualitative. Future low-temperature gate-doping experiments [32] for independently changing the electron-phonon coupling can be performed to quantify the importance of electron-phonon in Γ_G, as contrasted to other possible structural effects [5, 6]. The results might be unique as compared with similar works on single and AB-bilayer graphene [32, 33, 35], since in rTBG the electronic structure near the Fermi level is more complex, and switching the coupling off may not be achievable. In that way, it would be possible to use the micro-Raman spectra to evaluate twist-angle disorder [15] in rTBGs and for searching regions close to the magic angle.

In closing, we stress that twisted bilayer graphene (TBG) has drawn increasing attention since the discovery of strongly correlated phenomena, such as unconventional superconductivity [9]. In that context, the results shown here provide invaluable information on how local lattice vibration and electron-phonon coupling behaves in systems characterized by a soliton network such as rTBG. The presented findings rely on state-of-the-art developments in nano-Raman techniques and in computational and algorithmic developments that allow, for the first time, the accurate description of localization of phononic properties at length scales relevant to experiment. Our findings shed light on the importance of changes in the local density of states in the fundamental properties of rTBG at angles small enough to support the formation of soliton domains, important not only as a basis to understanding many-body effects but also to the outstanding optical, mechanical, thermal, and electronic properties common to graphene-related systems, but unique here due to the localization in the special rBLG system. Future advances would require the rigorous evaluation of electron-phonon coupling matrix elements. Given the size of the systems considered here, these cannot be directly computed without further algorithmic and theoretical developments. It is likely they will pave the way towards an understanding of such effects as Jahn-Teller effects [11] or electronic Cooper-like pairing [12–14]. Experimentally, this achievement was only conceivable because of the new tear-and-stack TBG preparation method and the use of plasmon-tunable tip pyramids [22] for tip-enhanced Raman spectroscopy that, at this point, is limited to transparent substrates (see Methods). In general, this work provides an important tool for the study of twistronics, with an extra degree of manipulation [16] of many quantum properties and exotic phenomena absent in pristine graphene, like ferromagnetism [38], anomalous quantum Hall effect [39] and large linear-in-temperature resistivity [40], and it may be useful for characterizing devices [15]. All these new aspects come with the ability,

presented here, to observe a crystallographic moiré pattern using visible light, and providing a full Raman spectrum for each image pixel.

METHODS

Theory

Phonons are computed using a combination of second-generation REBO potential for intralayer interactions and the registry-dependent Kolmogorov–Crespi (KC) potential, in its local normal formulation for intralayer interactions as fully described in Ref. [6]. For rTBG, relaxation of the structure in an energy-minimum microstate is crucial for an accurate description of its properties, and here all atomic positions and lattice parameters of the considered structures are optimized until all force components are less than 10^{-3} eV/atom. The dynamical force constants at the zone center are computed using finite differences. While our method is able to investigate (and unfold) phonons in tBLG structures made of tens of thousands of atoms, we are not able to reach structures with twist angles smaller than $\theta \sim 0.9°$, as the system size becomes prohibitively large in terms of diagonalization of the dynamical matrix, impinging affordable cost to computer memory, rather than CPU time.

The electronic structure is computed by diagonalizing a tight-binding Hamiltonian based on the recursive Green's function techniques that enables computing the real-space and momentum dependent local density of electronic states LDOS(E,$\mathbf{r}$,$\mathbf{k}$) of rTBG with extremely small angles (i.e. large moiré superlattices). This efficient numerical technique allows to calculate both local and total DOS using the same data from the fully-relaxed structure utilized for phonon calculations, and to present the electronic structure of rTBG using real/momentum space maps. More details in the supplementary information.

Optical setup

The nano-Raman system is a combination of a micro-Raman and a scanning probe microscopy setups in a TERS configuration, as described in [41], where the radially polarized light reaches the sample and the tip coming from an inverted optical microscope (thus limited

to transparent substrates [42]), tightly focused by an oil-immersion objective (1.4 numerical aperture), and the back-scattered light is collected by a spectrometer equipped with a charged-couple device (CCD). The TERS tips utilized are monopole-based plasmon-tunable tip pyramids, with nanopyramid size of $L = 470\,\mathrm{nm}$, which is resonant with the HeNe excitation laser (633 nm), generating an unusually high local enhancement, enough to surpass significantly the Raman signal coming from the considerably larger confocal illumination area [43]. This nano-antenna was produced as described in [22], with an apex diameter of 10 nm, as measured by scanning electron microscopy, generating a TERS resolution in the order of 20 nm, as observed in our data. The experiments are conducted in ambient conditions, with excitation laser power limited at 0.15 mW to avoid TERS tip burning and accumulation times limited at 0.5 s per spectrum to avoid too long hyperspectral TERS acquisitions.

Sample preparation

We prepared the rTBG samples by a new dry tear-and-stack method, using a Polydimethylsiloxane (PDMS) semi-pyramidal stamp covered with a polycarbonate (PC) sheet. The method is similar to the standard tear-and-stack [23], but here we use the PDMS stamp itself to tear a graphene flake in two pieces and stack them together, forming the rTBG arrangement. Next, we dry-transfer the rTBG from the stamp to a hexagonal boron nitride (hBN) flake, a flat substrate that is sufficiently decoupled from the sample [44], thus avoiding vibrational interference, reducing the surface roughness and improving the cleanliness of the sample. We do not heat the PC in this process to avoid contamination residues, we just make physical contact between the rTBG and hBN flakes, thus obtaining clean TBG without further sample annealing. See Fig. S1 for more details.

Data analysis

While the images in Figs. 1**d,e** were build directly from the spectral G′ band intensity and the G band linewidth, the AA and SP images in Figs. 2**d,e** relied on principal component analysis (PCA) due to the low signal-to-noise ratio observed for these weak features. PCA generated the representative features displayed in Figs. 2**f,g**, and each spectra of the corre-

sponding hyperspectral data was fit with a linear combination of the representative features. The fitted spectrum was confirmed to properly represent the feature signature by computing the Pearson's correlation between the raw data and the fitted profile. The contribution plot in Figs. 2**d,e** are defined by the percentile values of these linear coefficients. Contribution in Figs.3**c,d** follow the same definition with respect to the spectral features in Figs.3**a,b**.

References

[1] Jonathan S Alden, Adam W Tsen, Pinshane Y Huang, Robert Hovden, Lola Brown, Jiwoong Park, David A Muller, and Paul L McEuen. Strain solitons and topological defects in bilayer graphene. *Proceedings of the National Academy of Sciences*, 110(28):11256–11260, 2013.

[2] Xianqing Lin, Dan Liu, and David Tománek. Shear instability in twisted bilayer graphene. *Physical Review B*, 98(19):195432, 2018.

[3] Hyobin Yoo, Rebecca Engelke, Stephen Carr, Shiang Fang, Kuan Zhang, Paul Cazeaux, Suk Hyun Sung, Robert Hovden, Adam W Tsen, Takashi Taniguchi, et al. Atomic and electronic reconstruction at the van der waals interface in twisted bilayer graphene. *Nature materials*, 18(5):448–453, 2019.

[4] Lili Jiang, Zhiwen Shi, Bo Zeng, Sheng Wang, Ji-Hun Kang, Trinity Joshi, Chenhao Jin, Long Ju, Jonghwan Kim, Tairu Lyu, et al. Soliton-dependent plasmon reflection at bilayer graphene domain walls. *Nature materials*, 15(8):840–844, 2016.

[5] Alexandr I Cocemasov, Denis L Nika, and Alexander A Balandin. Phonons in twisted bilayer graphene. *Physical Review B*, 88(3):035428, 2013.

[6] Michael Lamparski, Benoit Van Troeye, and Vincent Meunier. Soliton signature in the phonon spectrum of twisted bilayer graphene. *2D Materials*, 7(2):025050, 2020.

[7] Ado Jorio and Luiz Gustavo Cançado. Raman spectroscopy of twisted bilayer graphene. *Solid State Communications*, 175:3–12, 2013.

[8] GSN Eliel, MVO Moutinho, AC Gadelha, A Righi, LC Campos, HB Ribeiro, Po-Wen Chiu, K Watanabe, T Taniguchi, Pascal Puech, et al. Intralayer and interlayer electron–phonon interactions in twisted graphene heterostructures. *Nature communications*, 9(1):1–8, 2018.

[9] Yuan Cao, Valla Fatemi, Shiang Fang, Kenji Watanabe, Takashi Taniguchi, Efthimios Kaxiras, and Pablo Jarillo-Herrero. Unconventional superconductivity in magic-angle graphene superlattices. *Nature*, 556(7699):43–50, 2018.

[10] Feng Shao and Renato Zenobi. Tip-enhanced raman spectroscopy: principles, practice, and applications to nanospectroscopic imaging of 2d materials. *Analytical and bioanalytical chemistry*, 411(1):37–61, 2019.

[11] Mattia Angeli, Erio Tosatti, and Michele Fabrizio. Valley jahn-teller effect in twisted bilayer graphene. *Physical Review X*, 9(4):041010, 2019.

[12] Fengcheng Wu, AH MacDonald, and Ivar Martin. Theory of phonon-mediated superconductivity in twisted bilayer graphene. *Physical review letters*, 121(25):257001, 2018.

[13] Fengcheng Wu, Euyheon Hwang, and Sankar Das Sarma. Phonon-induced giant linear-in-t resistivity in magic angle twisted bilayer graphene: Ordinary strangeness and exotic superconductivity. *Physical Review B*, 99(16):165112, 2019.

[14] Biao Lian, Zhijun Wang, and B Andrei Bernevig. Twisted bilayer graphene: A phonon-driven superconductor. *Physical review letters*, 122(25):257002, 2019.

[15] A Uri, S Grover, Y Cao, JA Crosse, K Bagani, D Rodan-Legrain, Y Myasoedov, K Watanabe, T Taniguchi, P Moon, et al. Mapping the twist-angle disorder and landau levels in magic-angle graphene. *Nature*, 581(7806):47–52, 2020.

[16] Eugene J Mele. Commensuration and interlayer coherence in twisted bilayer graphene. *Physical Review B*, 81(16):161405, 2010.

[17] Akio Yoshimori and Yoshiharu Kitano. Theory of the lattice vibration of graphite. *Journal of the Physical Society of Japan*, 11(4):352–361, 1956.

[18] Fernando Gargiulo and Oleg V Yazyev. Structural and electronic transformation in low-angle twisted bilayer graphene. *2D Materials*, 5(1):015019, nov 2017.

[19] F. Tuinstra and J. L. Koenig. Raman Spectrum of Graphite. *The Journal of Chemical Physics*, 53(3):1126–1130, 1970.

[20] Mildred S. Dresselhaus, Ado Jorio, Mario Hofmann, Gene Dresselhaus, and Riichiro Saito. Perspectives on carbon nanotubes and graphene Raman spectroscopy. *Nano Letters*, 10(3):751–758, 2010.

[21] Andrea C. Ferrari and Denis M. Basko. Raman spectroscopy as a versatile tool for studying the properties of graphene. *Nature Nanotechnology*, 8(4):235–246, 2013.

[22] Thiago L. Vasconcelos, Bráulio S. Archanjo, Bruno S. Oliveira, Rogério Valaski, Rafael C. Cordeiro, Helton G. Medeiros, Cassiano Rabelo, Aroldo Ribeiro, Peter Ercius, Carlos A. Achete, Ado Jorio, and Luiz Gustavo Cançado. Plasmon-Tunable Tip Pyramids: Monopole Nanoantennas for Near-Field Scanning Optical Microscopy. *Advanced Optical Materials*, 6(20):1800528, 2018.

[23] Kyounghwan Kim, Matthew Yankowitz, Babak Fallahazad, Sangwoo Kang, Hema C. P. Movva, Shengqiang Huang, Stefano Larentis, Chris M. Corbet, Takashi Taniguchi, Kenji Watanabe, Sanjay K. Banerjee, Brian J. LeRoy, and Emanuel Tutuc. van der waals heterostructures with high accuracy rotational alignment. *Nano Letters*, 16(3):1989–1995, 2016. PMID: 26859527.

[24] S. S. Sunku, G. X. Ni, B. Y. Jiang, H. Yoo, A. Sternbach, A. S. McLeod, T. Stauber, L. Xiong, T. Taniguchi, K. Watanabe, P. Kim, M. M. Fogler, and D. N. Basov. Photonic crystals for nano-light in moiré graphene superlattices. *Science*, 362(6419):1153–1156, 2018.

[25] Liangbo Liang, Alexander A Puretzky, Bobby G Sumpter, and Vincent Meunier. Interlayer bond polarizability model for stacking-dependent low-frequency raman scattering in layered materials. *Nanoscale*, 9(40):15340–15355, 2017.

[26] C Thomsen and S Reich. Double resonant raman scattering in graphite. *Physical review letters*, 85(24):5214, 2000.

[27] Andrea C Ferrari, JC Meyer, V Scardaci, C Casiraghi, Michele Lazzeri, Francesco Mauri, S Piscanec, Da Jiang, KS Novoselov, S Roth, et al. Raman spectrum of graphene and graphene layers. *Physical review letters*, 97(18):187401, 2006.

[28] Ji Eun Lee, Gwanghyun Ahn, Jihye Shim, Young Sik Lee, and Sunmin Ryu. Optical separation of mechanical strain from charge doping in graphene. *Nature Communications*, 3(May):1024, 2012.

[29] Jakob Zabel, Rahul R. Nair, Anna Ott, Thanasis Georgiou, Andre K. Geim, Kostya S. Novoselov, and Cinzia Casiraghi. Raman spectroscopy of graphene and bilayer under biaxial strain: Bubbles and balloons. *Nano Letters*, 12(2):617–621, 2012.

[30] Christoph Neumann, Sven Reichardt, Pedro Venezuela, Marc Drögeler, Luca Banszerus, Michael Schmitz, Kenji Watanabe, Takashi Taniguchi, Francesco Mauri, Bernd Beschoten, et al. Raman spectroscopy as probe of nanometre-scale strain variations in graphene. *Nature communications*, 6(8429):1–7, 2015.

[31] S Piscanec, M Lazzeri, Francesco Mauri, AC Ferrari, and J Robertson. Kohn anomalies and electron-phonon interactions in graphite. *Physical review letters*, 93(18):185503, 2004.

[32] Michele Lazzeri and Francesco Mauri. Nonadiabatic kohn anomaly in a doped graphene monolayer. *Phys. Rev. Lett.*, 97:266407, Dec 2006.

[33] Simone Pisana, Michele Lazzeri, Cinzia Casiraghi, Kostya S. Novoselov, A. K. Geim, Andrea C. Ferrari, and Francesco Mauri. Breakdown of the adiabatic born–oppenheimer approximation in graphene. *Nature Materials*, 6(3):198–201, 2007.

[34] J. C. Charlier, P. C. Eklund, J. Zhu, and A. C. Ferrari. Electron and phonon properties of graphene: Their relationship with carbon nanotubes. *Topics in Applied Physics*, 111(2008):673–709, 2008.

[35] A Das, B Chakraborty, S Piscanec, S Pisana, AK Sood, and AC Ferrari. Phonon renormalization in doped bilayer graphene. *Physical Review B*, 79(15):155417, 2009.

[36] H.B. Ribeiro, K. Sato, G.S.N. Eliel, E.A.T. [de Souza], Chun-Chieh Lu, Po-Wen Chiu, R. Saito, and M.A. Pimenta. Origin of van hove singularities in twisted bilayer graphene. *Carbon*, 90:138 – 145, 2015.

[37] Michele Lazzeri, Stefano Piscanec, Francesco Mauri, AC Ferrari, and J Robertson. Phonon linewidths and electron-phonon coupling in graphite and nanotubes. *Physical review B*, 73(15):155426, 2006.

[38] Aaron L. Sharpe, Eli J. Fox, Arthur W. Barnard, Joe Finney, Kenji Watanabe, Takashi Taniguchi, M. A. Kastner, and David Goldhaber-Gordon. Emergent ferromagnetism near three-quarters filling in twisted bilayer graphene. *Science*, 365(6453):605–608, 2019.

[39] M. Serlin, C. L. Tschirhart, H. Polshyn, Y. Zhang, J. Zhu, K. Watanabe, T. Taniguchi, L. Balents, and A. F. Young. Intrinsic quantized anomalous hall effect in a moiré heterostructure. *Science*, 367(6480):900–903, 2020.

[40] Hryhoriy Polshyn, Matthew Yankowitz, Shaowen Chen, Yuxuan Zhang, K. Watanabe, T. Taniguchi, Cory R. Dean, and Andrea F. Young. Large linear-in-temperature resistivity in twisted bilayer graphene. *Nature Physics*, 15(10):1011–1016, 2019.

[41] Cassiano Rabelo, Hudson Miranda, Thiago L. Vasconcelos, Luiz Gustavo Cancado, and Ado Jorio. Tip-enhanced Raman Spectroscopy of Graphene. In *2019 4th International Symposium on Instrumentation Systems, Circuits and Transducers (INSCIT)*, pages 1–6. IEEE, 2019.

[42] Hudson Miranda, Cassiano Rabelo, Luiz Gustavo Cançado, Thiago L Vasconcelos, Bruno S Oliveira, Florian Schulz, Holger Lange, Stephanie Reich, Patryk Kusch, and Ado Jorio. Impact of substrate on tip-enhanced raman spectroscopy: A comparison between field-distribution simulations and graphene measurements. *Physical Review Research*, 2(2):023408, 2020.

[43] Hudson Miranda, Cassiano Rabelo, Thiago L Vasconcelos, Luiz Gustavo Cançado, and Ado Jorio. Optical properties of plasmon-tunable tip pyramids for tip-enhanced raman spectroscopy. *physica status solidi (RRL)–Rapid Research Letters*, page 2000212, 2020.

[44] CR Woods, L Britnell, A Eckmann, RS Ma, JC Lu, HM Guo, X Lin, GL Yu, Y Cao, RV Gorbachev, et al. Commensurate–incommensurate transition in graphene on hexagonal boron nitride. *Nature physics*, 10(6):451–456, 2014.

Acknowledgments

This work was supported by CNPq (302775/2018-8 and INCT/Nanomaterials de Carbono), CAPES (RELAII and 88881.198744/2018-01) and FAPEMIG, Brazil. V-H.N. and J.-C.C. acknowledge financial support from the Fédeération Wallonie-Bruxelles through the ARC on 3D nano-architecturing of 2D crystals (16/21-077), from the European Union's Horizon 2020 Research Project and Innovation Program — Graphene Flagship Core3 (881603), from the Flag-Era JTC projects "MECHANIC" (R.50.07.18) and "TATTOOS" (R.8010.19), from the Belgium FNRS through the research projects (T.1077.15 & T.0051.18), and from the Francqui-Stichting Foundation. V.M., M.L acknowledge support from NY State Empire State Development's Division of Science, Technology and Innovation (NYSTAR).

Competing financial interests

The authors declare no competing financial interests

Authors contributions

Sample preparation: Andreij C. Gadelha, Daniel Miranda, Fabiano C. Santana, Eliel G. S. Neto, Jessica S. Lemos, Leonardo C. Campos, Rafael B. Nadas, Vinícius Ornelas; K. Watababe and T. Taniguchi provide hBN crystals; **Nano-Raman measurements:** Andreij

C. Gadelha, Cassiano Rabelo, Thiago L. Vasconcelos; **Micro-Raman measurements:** Andreij C. Gadelha, Eliel G. S. Neto, Jéssica S. Lemos, Rafael Nadas; **SPM measurements:** Douglas A. A. Ohlberg, Gilberto Medeiros-Ribeiro; **Phonon Structure Computation:** Benoit van Troeye, Michael Lamparski, Vincent Meunier; **Electronic Structure Computation:** Dawid Paszko, Viet-Hung Nguyen, Jean-Christophe Charlier; **Data Analysis:** Ado Jorio, Andreij C. Gadelha, Cassiano Rabelo, Eliel G. S. Neto, João L. Campos; **Project idealization and guidance:** Ado Jorio, Gilberto M. Ribeiro, Luiz G. Cançado, Leonardo C. Campos, Vincent Meunier; **Paper writing:** Ado Jorio, Andreij C. Gadelha, Vincent Meunier. Some authors contributed with parts of the text and figures, and they all read and agreed on the final version of the manuscript.

Author Information

Correspondence and requests for materials should be addressed to Ado Jorio (adojorio@fisica.ufmg.br) and Vincent Meunier (meuniv@rpi.edu).